Investigating the ability of astrocytes to drive neural network synchrony

Gregory Handy[1,2*], Alla Borisyuk[3*]

1 Departments of Neurobiology and Statistics, University of Chicago, Chicago, Illinois, USA
2 Grossman Center for Quantitative Biology and Human Behavior, University of Chicago, Chicago, Illinois, USA
3 Department of Mathematics, University of Utah, Salt Lake City, Utah, USA

*Corresponding authors: borisyuk@math.utah.edu, ghandy@uchicago.edu

Abstract

Recent experimental works have implicated astrocytes as a significant cell type underlying several neuronal processes in the mammalian brain, from encoding sensory information to neurological disorders. Despite this progress, it is still unclear how astrocytes are communicating with and driving their neuronal neighbors. While previous computational modeling works have helped propose mechanisms responsible for driving these interactions, they have primarily focused on interactions at the synaptic level, with microscale models of calcium dynamics and neurotransmitter diffusion. Since it is computationally infeasible to include the intricate microscale details in a network-scale model, little computational work has been done to understand how astrocytes may be influencing spiking patterns and synchronization of large networks. We overcome this issue by first developing an "effective" astrocyte that can be easily implemented to already established network frameworks. We do this by showing that the astrocyte proximity to a synapse makes synaptic transmission faster, weaker, and less reliable. Thus, our "effective" astrocytes can be incorporated by considering heterogeneous synaptic time constants, which are parametrized only by the degree of astrocytic proximity at that synapse. We then apply our framework to large networks of exponential integrate-and-fire neurons with various spatial structures. Depending on key parameters, such as the number of synapses ensheathed and the strength of this ensheathment, we show that astrocytes can push the network to a synchronous state and exhibit spatially correlated patterns.

Introduction

Recent theoretical work on neural circuits has successfully begun linking network structure to their underlying dynamics [1]. In particular, it has been shown that the statistics of connectivity (e.g., spatial scales of recurrent connectivity) can be used to predict the statistics of spiking behavior (e.g, level of network correlation) [2–4]. As reconstruction methods such as electron microscopy start to provide considerable amounts of data pertaining to the connectome of extensive brain regions [5–7], such theoretical work can guide the analysis of these massive datasets, suggesting the most useful network statistics to examine first. In this work, we develop a framework that extends computational spiking networks to efficiently include astrocytes, a non-neuronal

cell that is often included in such reconstructed volumes [8]. As a result, this method allows for improving the scope and accuracy of theoretical predictions linking network structure to network dynamics.

While the overwhelming majority of computational networks only account for conventional synaptic connections across excitatory and inhibitory populations of neurons, many synapses found *in vivo* are ensheathed, or tightly wrapped around, by astrocytes [9, 10]. It is well-known that astrocytes are engaged in bidirectional communication with nearby neurons, with recent breakthrough results demonstrating that astrocytes reliably encode sensory information [11]. Such communication is thought to occur through multiple pathways, such as neurotransmitter removal from the synaptic cleft, altering of extracellular ion concentrations, and the release of neuroactive substances [12–14]. The tightness of the ensheathment modulates the amount of extracellular space available around the synaptic site, and, as a result, is likely one of the contributing factors determining the properties of the synaptic connections and the overall dynamics of the network. However, it is unclear how one may explore these factors computationally, as the field currently lacks an efficient method to implement such micro-scale details into a large spiking network.

Further, the presence of ensheathed and non-ensheathed synapses in a network would require a higher degree of heterogeneity than considered previously, since modeling efforts have largely focused on networks with weak heterogeneities across key synaptic parameter values to none at all [15–18]. Here, synaptic parameters would need to be drawn from distinct distributions depending on the presence of an astrocyte. Interestingly, it has been experimentally shown that the number of synapses ensheathed by astrocytes differs dramatically between brain regions (e.g., 74% of cerebellar Purkinje cell synapses, 29% of the dendritic spines in the mouse visual cortex, and 60% of hippocampal synapses are ensheathed [9, 10]). Further, disease states such as epilepsy and Alzheimer's disease are known to have an increased number of hypertrophic astrocytes, known as reactive astrocytes [19, 20]. While reactive astrocytes vary in a number of ways from non-reactive astrocytes, their swollen structures imply a much tighter level of ensheathment. Taken together, synaptic ensheathment by astrocytes is a source of heterogeneity in synaptic connections that needs to be accounted for to make possible predictions as to how neuronal dynamics shift across brain regions and states. Interestingly, this concept has not been included in previous mathematical studies that have investigate the so-called "tripartite synapse" (pre- and post-synaptic terminals plus neighboring astrocyte, choosing to assume the astrocyte portion does not vary from synapse to synapse [21–24].

Despite the wealth of evidence for synaptic ensheathment, the role it might play in regulating brain activity is unknown. For example, enhanced synaptic ensheathment during epilepsy in hippocampal CA3-CA1 network might be contributing to the run-away excitability and to seizures, or, conversely, they might be playing a compensatory, protective role [25]. We use computational modeling at different spatial scales to differentiate between these two options, and, more generally, to take a step towards understanding the role of astrocyte ensheathment in altering network dynamics.

As mentioned above, astrocytes have many pathways of interacting with neurons. In this work we limit ourselves to only considering two such interaction pathways, namely, the physical barrier around the synapses presented by astrocyte wrapping and a rapid removal of neurotransmitter from the synaptic cleft by glutamate transporters on the surface of astrocyte. Building on our earlier work on detailed synaptic models [26, 27], we show that the ensheathed synapse can be thought of as faster and weaker than the same synapse without tight wrapping by an astrocyte. This allows us to create an "effective astrocyte ensheathment" model, which can be included in established neuronal network frameworks with only minimal increases in computational cost. Namely, an

"effectively ensheathed" synapse is endowed with parameter values (synaptic time constant and synaptic strength) derived from detailed studies of a synapse at the microscopic level. These synaptic properties are considered as parameterized only by the degree of astrocytic proximity at that synapse. This approach allows us to reevaluate several important examples of neuronal networks in which the dynamics had been well-studied and understood in the absence of astrocytes. We endow some of the individual synapses with "effective astrocyte ensheathment" by altering their synaptic parameters accordingly, and study the resulting changes in network dynamics.

We start in this work by analyzing simulations of the microscale DiRT (Diffusion with Recharging Traps) model for different levels of astrocyte protrusion into the synaptic cleft. This model finds a strong negative linear relationship between protrusion depth and the strength and time constant of the ensheathed synapse. In other words, astrocyte ensheathment leads to weaker and faster synaptic communication across neurons. We then implement this result into a series of large-scale spiking models similar to those studied extensively in [2]. This implementation transforms a homogeneous network, a network with uniform synaptic parameters across populations, into a heterogeneous network, where the parameter values for an individual synapse depend explicitly on its level of astrocyte ensheathment. We investigate the impacts this novel heterogeneity has on fundamental states of the network, such as its firing rate, pairwise correlation, and stability of its dynamic states. We demonstrate that, depending on key parameters, such as the number of synapses ensheathed and the degree of this ensheathment, astrocytes can push a non-spatial network from a balanced, asynchronous firing regime into a highly synchronous one. Consistently, we then show that when neuronal assemblies are embedded into our non-spatial network, astrocyte ensheathment can enhance correlations within populations. Finally, broadening our network architectures to include models with spatially structured connections, we find that these results readily extend, namely that the spatial correlation patterns sharpen (show stronger correlation in more spatially-restricted regions) in the presence of astrocytes.

Overall, our results indicate that our understanding of what dynamical modes can be expected from a particular network of neurons needs to be reevaluated in light of synaptic heterogeneity induced by astrocyte ensheathment. Specific ensheathment-induced parameter modification for individual synapses will need to be expanded as we learn more about the effects of the synaptic ensheathment from the detailed models. In the meantime, this framework can easily be applied to other dynamic networks in other contexts using our "effective ensheathment" approach.

Materials and methods

Exponential integrate-and-fire neuron

To examine the effects this type of ensheathment has on network level dynamics, we consider a two-layer network of exponential integrate-and-fire (EIF) neurons similar to the one used in [2]:

$$C_m \frac{dV_j^a}{dt} = I_L^a(V_j^a) + \psi^a(V_j^a) + I_j^a(t).$$

The first two terms on the right-hand side correspond to the leak

$$I_L^a(V) = -g_L^a(V - E_L^a),$$

and spike-generating current

$$\psi^a(V) = g_L^a \Delta_T^a \exp\left[\frac{V - V_T^a}{\Delta_T^a}\right],$$

respectively. The third term represents the synaptic input currents, and is given by

$$C_m^{-1} I_j^a(t) = F_j^a(t) + R_j^a(t),$$

where $F_j^a(t)$ represents the feedforward inputs and $R_j^a(t)$ are the recurrent inputs. We consider recurrent inputs of the form

$$R_j(t) = \sum_{b=e,i} \sum_{k=1}^{N_b} \frac{J_{jk}^{ab}}{\sqrt{N}} \left(\eta_b^{jk} * S_k^b \right)(t), \tag{1}$$

where $S_k^b(t)$ is the spike train, $\eta_b^{jk}(t)$ is the synaptic conductance of the following form

$$\eta_b^{jk}(t) = \frac{1}{\tau_b^{jk}} e^{-t/\tau_b^{jk}} \mathcal{H}(t), \tag{2}$$

and $\mathcal{H}(t)$ is the Heaviside function.

Connectivity and feedforward input

We consider both a randomly-connected recurrent layer and a spatially extended one. Unless otherwise noted in the figure captions, the parameter used for each network can be found in Tables 1-3.

Table 1. Out-degrees from population b (columns) to a (rows) for the non-spatial (spatial) model.

K_{ab}^{out}	E	I	Ffwd
E	2500 (2000)	2500 (2000)	N/A (10000)
I	2500 (500)	2500 (500)	N/A (800)

Non-spatial model

In the case of the non-spatial model, for each postsynaptic neuron in population b, we randomly and uniformly chose K_{eb}^{out} excitatory and K_{ib}^{out} inhibitory presynaptic neurons in the network (fixed-out degree) for it to be connected to. The random network receives feedforward inputs as smoothly varying input biases that can target specific subpopulations. Specifically, the feedforward input to each neuron was given by the sum of an input bias and a smoothly varying signal, $F_j^a(t)$

$$F_j^a(t) = \sqrt{N} m_a + \sigma_s s(t),$$

where $s(t)$ is smooth, unbiased Gaussian noise that is shared across neurons. We take its auto-covariance function to be

$$\text{cov}(s(t), s(t+\tau)) = \exp\left(-\frac{\tau}{2\tau_s^2} \right),$$

where τ_s sets the correlation timescale and σ_s scales the magnitude of the fluctuations. We consider two cases: 1) all neurons receive the same signal $s(t)$ (Fig 1A), and 2) half of the neurons received realization $s_1(t)$ and the other half received $s_2(t)$ (Fig 1B).

Table 2. Default parameter value for the non-spatial and spatial model (spatial model parameters in parentheses if different).

Parameter	Default value	Description
N_e	10,000 (40,000)	Number of excitatory neurons
N_i	10,000	Number of excitatory neurons
N_F	N/A (5,625)	Number of ffwd neurons
$\left[C_m^e/g_l^e, C_m^i/g_l^i\right]$	[15, 10] ms	membrane time constant
V_{th}	-10 mV	spike threshold
V_T	-50 mV	soft spike threshold
E_L	-60 mV	leak potential
V_{re}	-65 mV	reset threshold
$\left[\tau_{\text{ref}}^e, \tau_{\text{ref}}^i\right]$	[1.5, 0.5] ms	refractory time
$[\tau_e, \tau_i]$	[5, 4] ([6, 5]) ms	synaptic time constants
$\left[\Delta_T^e, \Delta_T^i\right]$	[2, 0.5] mV	EIF slope parameter
τ_s	40 (N/A) ms	Noise correlation timescale
$[m_e, m_i]$	[0.015, 0.01] (N/A) mV/ms	Static bias to ffwd input
σ_s	0.1 (N/A) mV/ms	noise fluctuations magnitude
r_F	N/A (5) Hz	Firing rate of ffwd neurons

Table 3. Default synaptic strength from population b (columns) to a (rows) for the non-spatial (spatial) model.

J_{ab}	E	I
E	12.5 (40)	50 (400)
I	20 (120)	50 (400)

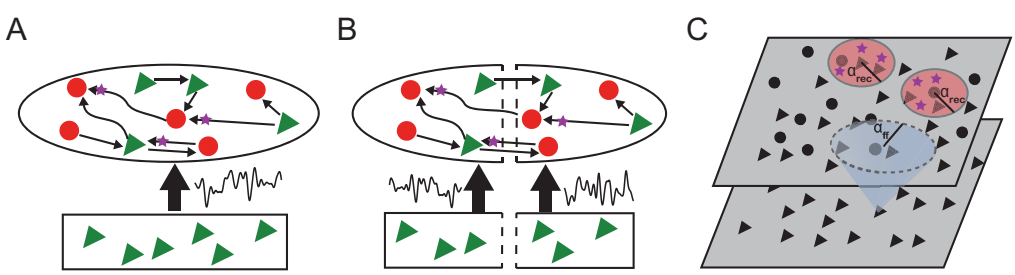

Fig 1. Network schematics. We consider networks of excitatory (green triangles) and inhibitory (red circles) neurons with different connectivity rules. Individual synapses can be ensheathed by an astrocyte (purple stars). A: One population, non-spatial network where all neurons receive the same Gaussian noise $s(t)$. B: Two population, non-spatial network where the neurons are randomly split to either receive $s_1(t)$ or $s_2(t)$. C. Spatial network on a periodic domain, where the recurrent connections can be ensheathed by astrocytes.

Spatial model

To model the spatial network, we arranged N_e excitatory and N_i inhibitory neurons on a uniform grid covering a two-dimensional square domain (Fig 1C). Similarly, the

feedforward layer consisted of N_F excitatory neurons uniform grid covering a square that is parallel to the recurrent network. We then normalized each grid such that the domain lied in the unit square $\Gamma = [0,1] \times [0,1]$. Neurons were connected randomly and the probability that two neurons were connected depended on their distance measured periodically on Γ. We used the same algorithm presented in [2] to form the connections. Given a presynaptic neuron at coordinates $y = (y_1, y_2)$ in population b and a postsynaptic neuron at $x = (x_1, x_2)$ in population a, this algorithm creates a network where the expected number of synaptic contacts from a is given by

$$p_{ab}(x-y) = \frac{K_{ab}^{\text{out}}}{N_a} g(x_1 - y_1; \alpha_b) g(x_2 - y_2; \alpha_b) \tag{3}$$

where $g(u;\alpha)$ is a wrapped Gaussian distribution [28]. The N_F feedforward neurons are taken to be Poisson-spiking, so that the feedforward input to the recurrent layer is

$$F_j^a(t) = \sum_{k=1}^{N_F} \frac{J_{jk}^{aF}}{\sqrt{N}} \left(\eta_e * S_k^F\right)(t).$$

Microscale model of neurotransmitter diffusion

We use the diffusion with recharging traps (DiRT) model [26,27] to investigate the number of neurotransmitters that interact with receptors found on the postsynaptic terminal vs. those that diffuse out of the synaptic cleft and interact with the ensheathing astrocyte. We consider a similar idealized synapse as this previous work, taking the cleft to be a two-dimensional domain

$$\Omega^{\text{cleft}} = [0, c_w] \times [0, c_h],$$

where c_w is the width of the cleft, and c_h is the height. N_{rec} postsynaptic receptors of equal size are located along the postsynaptic density

$$\partial\Omega_{\text{rec}}^{\text{cleft}} = \{(x,y) | y = 0, x \in [\text{psd}_1, \text{psd}_2] \subseteq [0, c_w]\},$$

and the ensheathing astrocyte is taken to be

$$\partial\Omega_{\text{astro}} = \{(x,y) | x = p/2 \text{ and } x = c_w - p/2\},$$

where p is the amount of astrocyte protrusion (Fig 2A). Note that we also allow for a negative protrusion amount, in which case the domain outside of the cleft is referred to as the extracellular space Ω^{extra}.

The simulation begins with N_{NT} neurotransmitters being released at $(c_w/2, c_h)$. While in the cleft or in the extracellular space, the neurotransmitters diffuse according to

$$d\mathbf{X}_k(t) = \sqrt{2D} d\mathbf{W}_k(t), k = 1, ..., N_{\text{NT}} \text{ for } \mathbf{X}_k(t) \in \left(\Omega^{\text{cleft}} \cup \Omega^{\text{extra}}\right)$$

where $\mathbf{X}_k(t)$ denotes the location of the neurotransmitter, $\mathbf{W}_j(t)$ denotes independent Wiener processes, and D is the diffusion coefficient. The receptors along the postsynaptic terminal are taken to be partially absorbing, meaning the probability of a particle being absorbed upon making contact is

$$\text{Probability of absorption} = \frac{K\sqrt{\pi}}{\sqrt{D}} \sqrt{\Delta t},$$

where Δt is the time step of the diffusion model and K is the absorption rate. After absorbing a particle, the receptors recharge with a rate τ_r. The astrocyte boundary is taken to be a perfect absorber with no recharge. All parameter corresponding to this microscale model can be found in Table 4.

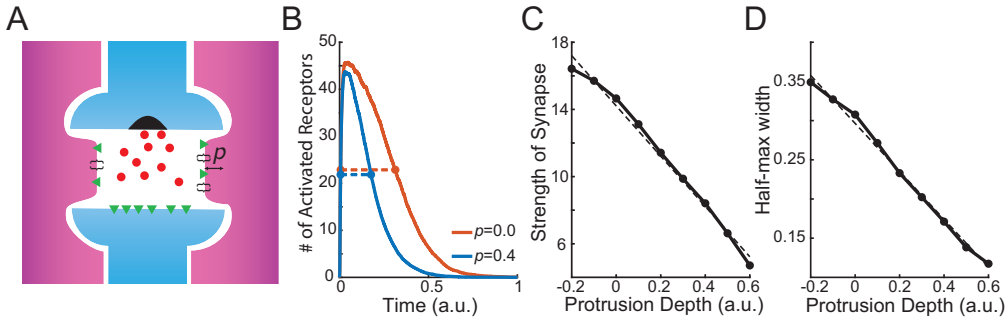

Fig 2. Model of astrocyte ensheathment. A: Schematic of astrocyte (purple) ensheathment of a synapse (blue). The astrocyte is protruding into the synaptic cleft by amount p. B: Time course of receptor activation in a diffusion with recharging traps simulation for different synaptic protrusion depths (red: $p = 0$, blue: $p = 0.4$) of the neighboring astrocyte, with the half-max widths denoted (dashed lines). C: Strength of synapse, defined as the area under the curve of activation time course, and D: half-max width as a function of protrusion depth. Line of best fit denoted by the dashed line (C: $R^2 = 0.9900$ and D: $R^2 = 0.9947$).

Table 4. Default parameter value for the DiRT model (arbitrary units).

Parameter	Default value	Description
N_{NT}	1000	Number of neurotransmitters released
N_{rec}	50	Number of postsynaptic receptors
τ_r	0.1	receptor recharge time
K	1	absorption rate
D	1	diffusion coefficient
c_w	1	cleft width
c_h	0.1	cleft height
$[\mathrm{psd}_1, \mathrm{psd}_2]$	[0.25 0.75]	postsynaptic density location
p	0	protrusion depth
Δt	0.00001	diffusion time step

Results

Modeling astrocyte ensheathment with an effective astrocyte

We start by investigating how absorption of excess neurotransmitter by astrocytes can shape synaptic time courses. After neurotransmitters are released into the synaptic cleft, they either interact with receptors on the postsynaptic terminal or are absorbed by neighboring astrocytes (e.g., via glutamate transporters). While it is reasonable to assume the depth that an astrocyte protrudes into a cleft impacts the number of neurotransmitters ending up in each destination, it is unclear whether this impact is enough to significantly alter the strength of the transmitted signal. To address this unknown, we make use of the DiRT model [26, 27] to simulate particles interacting the receptors on this microscale domain (Fig 2A). We find that the protrusion of an

astrocyte noticeably decreases the synaptic time course by effectively assisting the cleft in clearing out neurotransmitters (Fig 2B, red: $p = 0$, blue: $p = 0.4$). Further, by defining the strength of the synapse to be the area under the curve of these synaptic time courses, we find that that protrusion causes the synapse to become noticeably weaker. Considering a range of protrusion values ($p \in [-0.2, 0.6]$), reveals that the protrusion amount and the strength vary linearly (Fig 2C, $R^2 = 0.9900$), which also holds true for the half-max width (Fig 2D, $R^2 = 0.9947$).

Such microscale simulations are computationally intractable to conduct in a large network of spiking neurons, but they provide insight into how one might include "effective" astrocytes in such a model. Namely, a synapse that is ensheathed by an astrocyte should be weaker and faster than an unsheathed synapse. As a result, an ensheathed synapse should have smaller values for J and τ, which correspond to the synapse's strength and time constant respectively (see Eqs 1 and 2).

We implement the results of the microscale model by considering a synaptic connection from neuron k to neuron j and let $\mathbf{1}_{jk\ \text{ensheathed}}$ be an indicator function that equals 1 if the jk synapse is ensheathed, and zero otherwise. We then choose to set this synapse's strength J_{jk}^{ab} and time constant τ_b^{jk} to be

$$\begin{aligned} J_{jk}^{ab} &= J^{ab} \cdot \left(1 - (1 - s_{en}^{ab}) \cdot \mathbf{1}_{jk\ \text{ensheathed}}\right), \text{ and} \\ \tau_b^{jk} &= \tau_b \cdot \left(1 - (1 - s_{en}^{ab}) \cdot \mathbf{1}_{jk\ \text{ensheathed}}\right), \end{aligned}$$

where s_{en}^{ab} is the strength of the astrocyte ensheathment from population b and a. This model captures the key results from the DiRT simulations, namely the peak of the synaptic time course does not depend on ensheathment and it is a linear function of ensheathment strength (s_{en}^{ab} can be thought of as $1 - p$). To enforce the fact that ensheathed synapses are weaker and faster, we only consider $0 < s_{en}^{ab} < 1$. Lastly, the probability that a synapse from population b to a is ensheathed is given by p_{en}^{ab}.

The difference between this and previous network models that accounted for synaptic heterogeneity is that the synaptic strength J_{jk}^{ab} and synaptic time constant τ_b^{jk} of different synapses are highly variable across the network. Though this adjustment appears deceptively subtle, allowing each synapse to have its own synaptic parameters introduces a level of heterogeneity not seen in previous work. We investigate how this heterogeneity introduced by astrocyte ensheathment tunes the network's ability to synchronize in a number of different contexts: 1) non-spatial recurrent layer with a single smoothly varying input bias, 2) with two smoothly varying input bias sent to distinct populations, and 3) a spatial recurrent layer, receiving feedforward input from Poisson-spiking.

Astrocyte ensheathment can break E-I balance, causing synchronous activity

We start by considering a non-spatial recurrent layer with each neuron receiving the same smoothly varying signal $s(t)$ (Fig 1A). Such a network can exist in the asynchronous balanced state, as long as the network is placed in the appropriate parameter regime as derived in [2]. Placing our EIF network into such a regime yields the expected result, a network with asynchronous spiking (Fig 3A). However, introducing astrocyte ensheathment ($p_{\text{en}}^{ae} = 0.7$, $p_{\text{en}}^{ai} = 0$, $s_{en}^{ab} = 0.5$), while keeping the underlying connectivity matrix and feedforward input the same, broke E-I balance and caused the network to show strong levels of synchrony (Fig 3B and 3C). Interestingly, while both realizations of the neuronal network with astrocytes developed synchronous activity, they occurred at different time points.

To investigate what caused the balance state to be lost, we examine the normalized shared current across 500 neurons (Fig 4A; default: solid, dashed: realization 1,

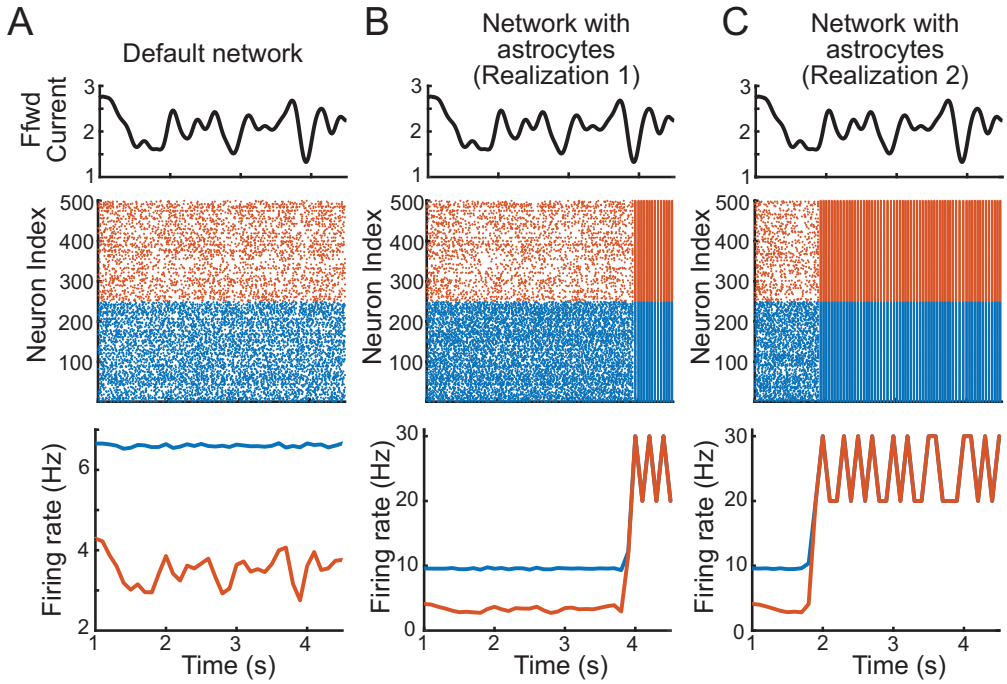

Fig 3. Astrocyte ensheathment can lead to synchronous firing across the network. A: The time course of the input current (top), spiking times of 500 sampled neurons (middle; blue: excitatory, red: inhibitory) from the one population, non-spatial network, and average firing rate (bottom) for the default network without astrocytes showing asynchronous firing rates. B and C: same but for two network with astrocytes realizations, with both networks exhibiting synchronous activity.

dot-dashed: realization 2). Initially we observe that the recurrent activity in all three networks tracks and cancels the feedforward input, the crucial characteristic of a balanced network (Fig 4A; gray lines). However, we see that this breaks down at around 1.8 seconds. At this time, the feedforward input into the networks significantly decreases, and the recurrent activity in second realization of the astrocyte network is unable to successfully cancel it. As a result, the balanced state is lost and the network transitions into synchronous firing.

In the balanced state, such a drop in the feedforward input is accompanied by an increase in the recurrent current. As seen in the dynamics of the default network (Fig 4B), this occurs with slight adjustments in the excitatory current, which are tracked by the inhibitory currents. However, both networks with astrocytes are unable to make such these fine tuned adjustments, which leads to growing oscillations in both the excitatory and inhibitory currents. These networks lost their ability to make this fast, fine tuned adjustments since their excitatory synapses have been ensheathed by an astrocyte. This ensheathment leads to excitatory synapses with faster time constants than the inhibitory ones. Such slow inhibition is known to result in synchronous behavior [29]. Eventually, the recurrent inhibition in the second network realization fails at containing the recurrent excitation, leading to the synchronous firing of almost all neurons in the network. However, due to random differences between realizations (i.e., the specific synapses chosen for astrocyte ensheathment), the first network realization is able to recover from this oscillatory behavior as the feedforward input begins to increase and maintain the balance state. Nonetheless, it fails later on in the simulation when the feedforward input decreases in a similar, although greater in magnitude, manner (S1 Fig).

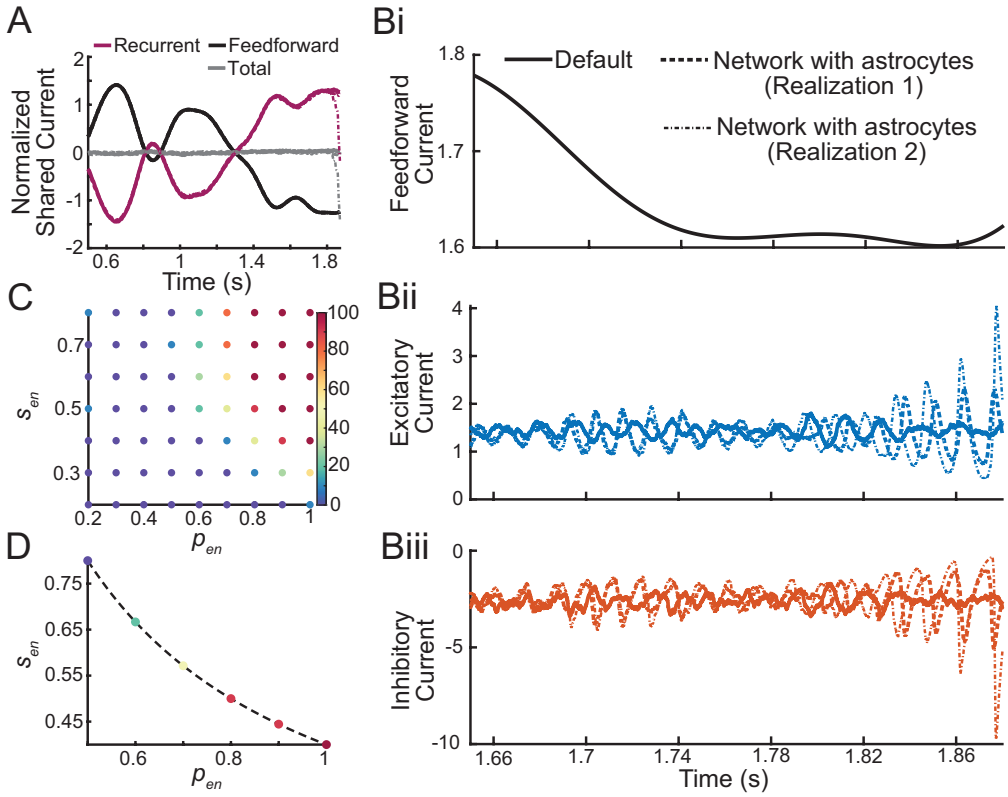

Fig 4. Astrocyte ensheathment can break E-I balance. A: Normalized shared fluctuations in the feedforward (black) and recurrent (purple) synaptic inputs for all three one population, non-spatial networks (solid: default; dashed: realization 1; dot-dashed: realization 2). Initially, all three networks have the recurrent and feedforward synaptic input canceling, leading to weak shared fluctuations (gray), until the balance state is lost in realization 2. The curves were computed by averaging the synaptic input currents to 500 neurons, convolving with a Gaussian-shaped kernel ($\sigma = 15$ ms), subtracting the mean and dividing by the neurons' rheobase. B: Shared fluctuations (not normalized) in the i) feedforward, ii) excitatory, and iii) inhibitory currents across realizations (solid: default; dashed: realization 1; dot-dashed: realization 2) zoomed in on the time window when the asynchronous state is lost in realization 2. C: Percent of the ten EIF networks that led to synchronous dynamics in 5 seconds of simulation as a function fo ensheathment parameters. D: The $\hat{s}_{en}^{ab} = s_{en}^{ab} \cdot p_{en}^{ae} = 0.4$ isoline showing that a naïve mean field approximation would fail at capture this phenomenon. Colorbar is the same as panel C.

In order to better understand how parameters underlying astrocyte ensheathment lead to synchronization, we consider ten default EIF networks, each with a different input signal $s(t)$ and no astrocyte ensheathment. These ten networks all exhibited asynchronous spiking solutions for the full length of the trial (taken to be 5 seconds). We then ask whether or not these same networks synchronized in the presence of astrocyte ensheathment. Discretizing the parameter space $p_{en}^{ae} \times s_{en}^{ab} = [0.1, 1] \times [0.2, 0.8]$ into seventy parameter sets, we observe that all ten networks eventually exhibit synchronous behavior as p_{en}^{ae} and s_{en}^{ab} increase (Fig 4C; red dots in upper right corner). However, we also observe that there is not a sharp transition point from blue (all networks remain in the asynchronous state) to red (all networks become synchronous). This suggests that for intermediate values of p_{en}^{ae} and s_{en}^{ab}, random differences in the connectivity diagram and the locations of astrocyte ensheathment are enough to prime some networks to tend toward synchrony over others.

These results highlight the shortcomings that a naïve mean field theory would have in capturing the dynamics brought on by this type of synaptic heterogeneity. More specifically, one might be tempted to simply average out the effect of astrocyte ensheathment across the network and adjust the strength of all synapses to be

$$\hat{s}_{en}^{ab} = s_{en}^{ab} \cdot p_{en}^{ae} + 0 \cdot (1 - p_{en}^{ae}) \,. \tag{4}$$

However, by considering the outcomes across the $\hat{s}_{en}^{ab} = 0.4$ iso-line (Fig 4D), the heterogeneous networks may rarely exhibit synchrony (low p_{en}^{ae}, high s_{en}^{ab}) or frequently (high p_{en}^{ae}, low s_{en}^{ab}).

Astrocyte ensheathment can enhance correlations already present within a network

The previous section explored how astrocyte ensheathment affects the dynamics of a balanced network operating in the asynchronous regime. Now we examine a similar non-spatial network, except now we allow for two subpopulations of neurons, where each subpopulation receives its own feedforward input (Fig 1B). As previously shown, such a network breaks the asynchronous state, with positive correlations among neurons from the same population and negative correlations across populations [2]. As a result, the correlation distribution becomes strongly binomial (Fig 5A,B; solid lines).

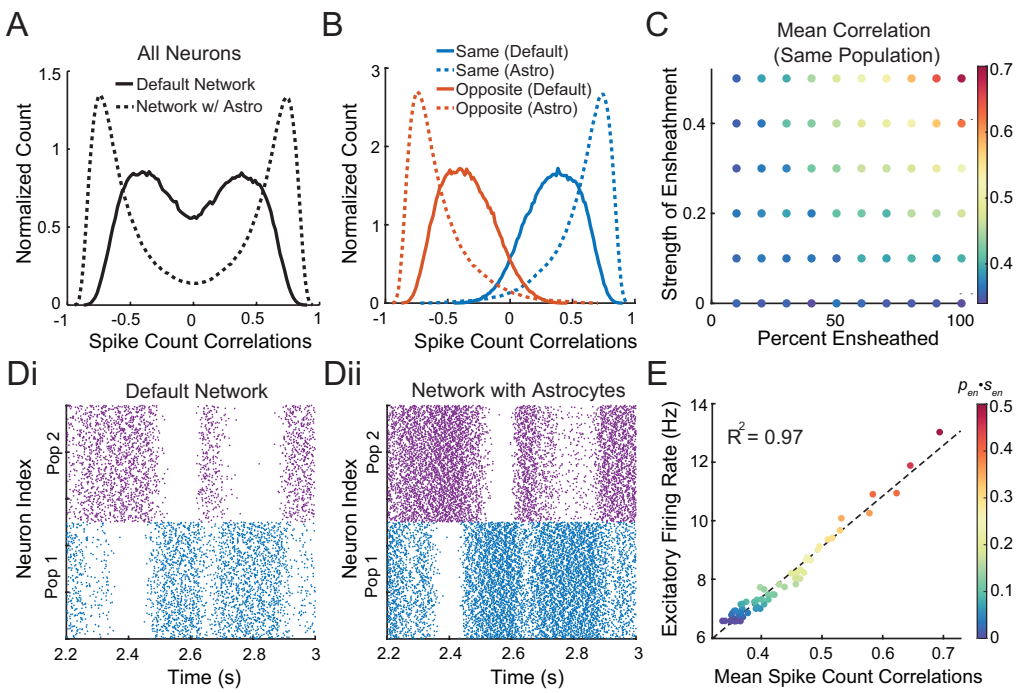

Fig 5. Astrocyte ensheathment can lead to greater correlations. A: Normalized histogram of pairwise spike count correlations between 1000 neurons for the default two population, non-spatial network (solid) and the same network with astrocytes (dashed), with parameters $(p_{en}, s_{en}) = (0.8, 0.5)$. B: Same as panel A, except the pairwise spike count correlations calculated within and across each populations. C: Mean pairwise spike count correlations within the same population as a function of ensheathment parameters. D: Raster plots for the two populations for the i) default network and ii) network with astrocytes $(p_{en}, s_{en}) = (0.8, 0.8)$. E: Mean spike count correlations plotted against the excitatory firing rate for different astrocyte conditions (the color of dots corresponds to $p_{en} \cdot s_{en}$ for that simulation).

Exploring a more subtle effect of astrocyte ensheathment than the previous section, we now consider astrocyte ensheathment that is agnostic to synapse type. Specifically, we consider the parameter space (p_{en}, s_{en}), where p_{en} is the probability of any synapse being ensheathed, and s_{en} is the strength of that ensheathment. Setting $p_{en} = 0.8$ and $s_{en} = 0.5$, we find that the binomial distribution of spike count correlations present in the default network becomes more extreme, with an increase in the positive correlation among the same population and a decrease in the negative correlations across populations (Fig 5A,B; dashed lines). This trend is true in general: as p_{en} and s_{en} increase, the correlations among a single population also increase (Fig 5C), while the correlations across different populations decrease (figure not shown).

To gain additional insight into how astrocytes are modulating the spiking behavior of the network, we compare the raster plot of the default network to a network with astrocytes, where both networks receive the same feedforward inputs (Fig 5D).

As expected from the earlier observation that there are negative correlations across populations (Fig 5B), the two populations show clear competitive dynamics. However, unlike the previous network configuration, the network with astrocytes doesn't qualitatively change the spiking behavior. Instead, it is clear from these raster plots that key quantitative traits, such as the times the dominate spiking populations switches, are largely conserved across networks.

One observable difference between the networks is the firing rate: the network with astrocytes appears to have a higher firing rate in both populations. Previous work [30] would suggest that this difference could be sufficient to explain the increase in correlations, and indeed, we find a strong ($R^2 = 0.97$) positive relationship between the spike count correlations and the excitatory firing rate, with higher fire rates arising with stronger astrocyte ensheathment (Fig 5E; color corresponding to $p_{en} \cdot s_{en}$). This strong relationship between firing rate, correlations and astrocyte ensheathment suggest that unlike the last network configuration, a mean-field model with parameter in Eq. 4 could be used to capture the effect of astrocytes on the neuronal dynamics. See Discussion for additional considerations regarding a mean-field approach.

Astrocytes enhance spatial correlations

We now consider the implementation of "effective" astrocytes in a spatial model (Fig 1C). Specifically, we arrange the recurrently connected neurons in a two dimensional grid, with a Gaussian connectivity profile (see Eq. 3), the spread of which is given by parameter α_{rec}. Unlike the previous sections, the feedforward inputs are provided by neurons that are Poisson-spiking. These neurons also lie on a two-dimensional grid and make connections based on a Gaussian connectivity profile with spread parameter α_{ff}. We consider astrocyte ensheathment of only recurrent excitatory synapses, but not inhibitory or feedforward ones.

In agreement with [2], we find that when the spatial profile of recurrent connections is less than the feedforward (i.e., $\alpha_{\text{rec}} < \alpha_{\text{ff}}$), the default network exists in an spatially asynchronous state, with small pairwise spike count correlations between neurons of any distance (Fig 6A, left and 6B, black). In fact, [2] proves that the asynchronous state requires $\alpha_{\text{rec}} < \alpha_{\text{ff}}$. However, by introducing astrocyte ensheathment to this model ($p_{en}^{ae} = 0.9$, $p_{en}^{ai} = 0$ and $s_{en} = 0.5$), we find that the asynchronous state can be broken without changing the spatial profiles of connectivity. Specifically, we observe strong positive correlations arising between nearby neurons and negative correlations from those farther away (Fig 6B, orange), resulting in tight clusters of spiking neurons (Fig 6A, right). However, these tight clusters do not persist across time (S1 Movie).

These results mirror those found in the non-spatial network with a single population of neurons (Fig 3), and arise from similar mechanisms. Specifically, astrocyte ensheathment speeds up excitatory synapses. As a result, the inhibitory synapses are

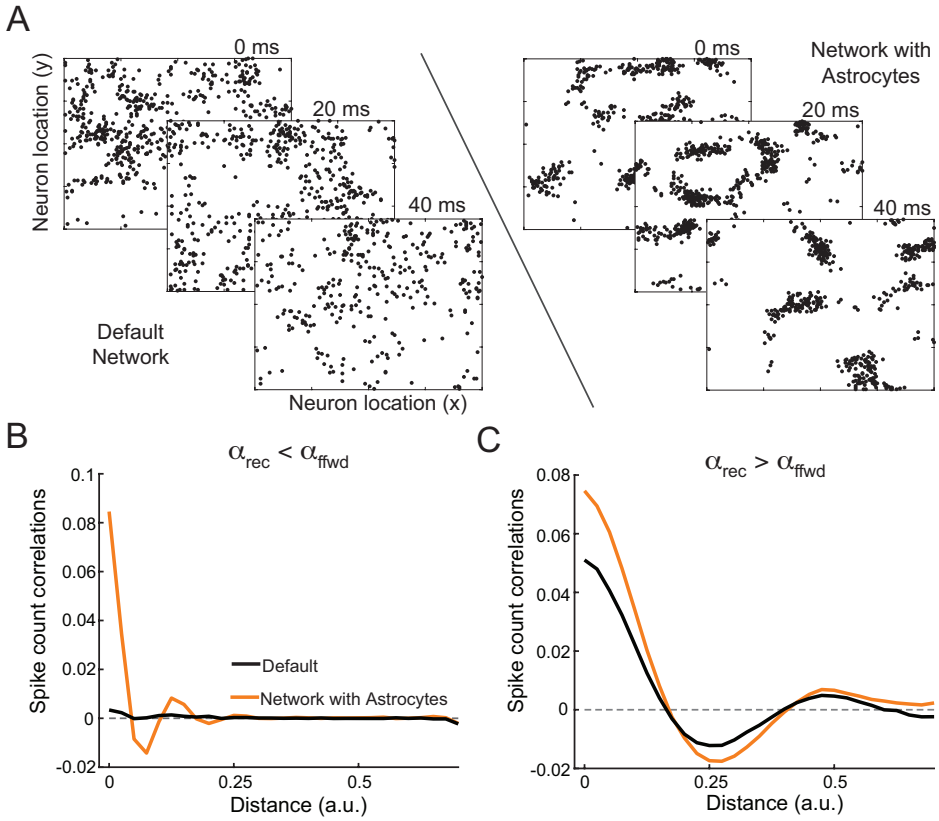

Fig 6. Astrocyte ensheathment can lead to greater spatial correlations. A: Spatial raster plots at three 20 msec time points for the default network (left) and network with astrocyte ensheathment (right). Parameters were chosen such that the default network exhibited no spatial correlations ($\alpha_{\rm rec} = 0.05$, $\alpha_{\rm ffwd} = 0.1$, and $(p^{ae}_{en}, p^{ai}_{en}, s_{en}) = (0.9, 0, 0.5)$). B: Spike count correlation plots as a function of distance between neuron pairs corresponding to the parameters in panel A for the default (black) and network with astrocytes (orange). C: Same as panel B, except with a default network placed in the spatial correlation regime ($\alpha_{\rm rec} = 0.2$, $\alpha_{\rm ffwd} = 0.1$, and $(p^{ae}_{en}, p^{ai}_{en}, s_{en}) = (0.8, 0, 0.5)$).

unable to track and cancel recurrent excitation, which leads to a loss of the asynchronous balance state. However, unlike our previous results corresponding to the non-spatial network, the network activity organizes in tight spatial patterns, as opposed the synchronous firing of the entire network.

In further agreement with [2], when the recurrent connection's spatial profile is larger than the feedforward projections (i.e., $\alpha_{\rm rec} > \alpha_{\rm ff}$), we find that the default network now exhibits spatial correlations (Fig 6C, black). In this case, astrocyte ensheathment of excitatory synapses does not qualitatively change this behavior, but instead simply enhances these spatial correlations at almost all distances (Fig 6C, orange), with the exception being the distances where spatial correlations are zero. This is true for a range of astrocyte ensheathment parameters: stronger astrocyte ensheathment, either through p_{en} or s_{en} leads to stronger spatial correlations, while not affecting the spatial footprint of these correlations (S2 Fig). In this case, with the balance state already broken due to the widths of the spatial projections, astrocyte ensheathment of excitatory synapses simply amplifies the inability of inhibitory neurons to track and cancel recurrent excitation at all spatial scales.

Discussion

Through microscale modeling of neurotransmitter diffusion, this work derives an efficient way to implement astrocytes ensheathment of synapses in large scale neuronal networks. Specifically, simulations on the microscale domain of the synaptic cleft suggested that ensheathed synapses are weaker and faster than their non-ensheathed counterparts. This investigation identified the synaptic strength and synaptic time constant as the key parameters to vary to denote the presence of an "effective" astrocyte.

Such parameters are commonly found in current- and conductance-based spiking networks with recurrent connections (e.g., [2, 31–34]), making the implementation presented here applicable to many network architectures and parameter regimes. Here, while we considered both non-spatial and spatial networks, we largely concerned ourselves with networks placed in the so-called "tight balanced" regime [35], and showed that astrocyte ensheathment can dramatically change firing dynamics, break the balance state, and cause synchronous behavior. While our network examples are classified as inhibition-stabilized networks (ISN), meaning the fixed point is stabilized by feedback inhibition, it is unclear which of our results extend to other ISNs, such as those in the "loose balance" regime (e.g., stabilized supralinear network) [35, 36]. For example, we were able to explain the synchronous firing in our non-spatial network (Fig. 3) as due to the astrocytes targeting and speeding up excitatory synapses, which the inhibitory currents were unable to track and cancel. In these other ISN frameworks, this tight canceling does not occur, so it is unclear if similar synchronous firing would arise. On the other hand, all ISN frameworks require sufficiently strong inhibition, so astrocytes targeting inhibitory neurons would lead to stability issues across all balanced regimes. Future work will push these lines of inquiry further, made easier in part by the straightforward implementation of our astrocyte framework.

The investigation of the balance state as a function of synaptic time courses was also completed recently in [31], but our work differs in a few notable areas. First, the adjustment of the synaptic time courses here arose from the implementation of astrocyte ensheathment around individual synapses. This resulted in a heterogeneous network, which behaves qualitatively differently than its homogeneous network counterpart found by a naïve mean field (see Fig 4). Second, we observed spatial patterns emerge in the $\alpha_{\text{rec}} < \alpha_{\text{ff}}$ regime when astrocyte ensheathment was present, showing that this condition, as derived in [2], is a necessary condition for the balance state, but not a sufficient one. Meanwhile [31] only considered homogeneous networks in the $\alpha_{\text{rec}} > \alpha_{\text{ff}}$ regime.

We also note that the heterogeneity introduced by astrocyte ensheathment considered here is significantly different than other models that consider heterogeneous parameters. For example, previous works have implemented heterogeneity in connection strengths by having the J^{ab}_{jk}'s be randomly distributed according to the normal distribution $\mathcal{N}(J, \sigma)$ [16–18], resulting in only small variations of parameters across the network. Here, the synaptic parameters corresponding to ensheathed and unsheathed synapses are pulled from entirely distinct distributions, specifically

$$(J^{ab}_{jk}, \tau_b^{jk}) \quad = \begin{cases} (J^{ab}, \tau_b) & \text{if synapse } k \to j \text{ is unsheathed} \\ (J^{ab} \cdot s^{ab}_{en}, \tau_b \cdot s^{ab}_{en}) & \text{if synapse } k \to j \text{ is ensheathed} \end{cases}.$$

This heterogeneity can also be extended further, either by considering distributions for the synaptic parameters as done in previous works, or by considering a distribution on the ensheathment parameter s^{ab}_{en}, which would allow various degrees of astrocyte ensheathment across a single network. We leave such investigations to future work.

Additionally, we found that it is non-trivial to capture this novel form of network heterogeneity in a mean-field approximation, complicating the extension of this framework to be included in rate-based models of average population dynamics.

Specifically, when we considered astrocyte ensheathment of excitatory synapses, we showed that a naïve mean-field theory (see Eq 4) would fail to capture key qualitative dynamics of the full model (Fig 4D). On the other hand, when we allowed astrocytes to equally ensheathed both excitatory and inhibitory synapses, we found a tight relationship between correlations, firing rates, and astrocyte ensheathment (Fig 5E), suggesting that a mean-field approximation in this parameter regime could be possible. So while a mean-field approach could work in the latter case, it would be interesting future work to investigate how robust such an approximation would be in the presence of symmetry breaking changes in parameters, either in the probability and/or strength of ensheathment.

Lastly, our model of astrocyte-neuron interaction only accounts for the ability of astrocyte to assist in the clearance of neurotransmitters from the synaptic cleft by acting as an effective buffer and transporter [12, 37]. However, these neurotransmitter may also activate receptors found on astrocyte membrane (e.g., mGluR5), leading to the activation of calcium pathways [38, 39]. While the downstream effects of this pathway are still being investigated, evidence suggests that it may impact other aspects of neuronal signaling not considered in this work, such as the overall excitability of the network by either adjusting the resting potential of neurons [40] or through the direct release of gliotransmitters [14] (but see [41–43]). Here, we show the unanticipated result that this calcium pathway is not needed for astrocytes to strongly tune network dynamics. They just need to be able to modulated how close they are to their neighboring neurons. However, future work should seek to connect these additional communication pathways to the ensheathment interaction investigated here to further advance our understanding.

Supporting information

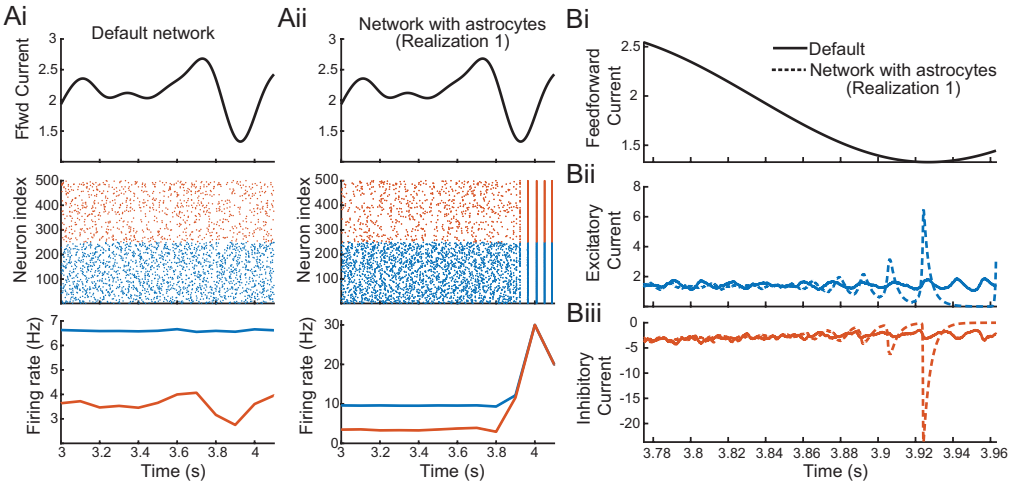

S1 Fig. Broken E-I balance in Realization 1. Ai: The time course of the input current (top), spiking times of 500 sampled neurons (middle; blue: excitatory, red: inhibitory), and average firing rate (bottom) for the default network without astrocytes showing asynchronous firing rates. Aii: Same but for network with astrocytes realization 1. B: Shared fluctuations in the i) feedforward, ii) excitatory, and iii) inhibitory currents across realizations (solid: default; dashed: realization 1) zoomed in on the time window when the asynchronous state is lost in realization 1. Same parameters as Fig 3 and 4.

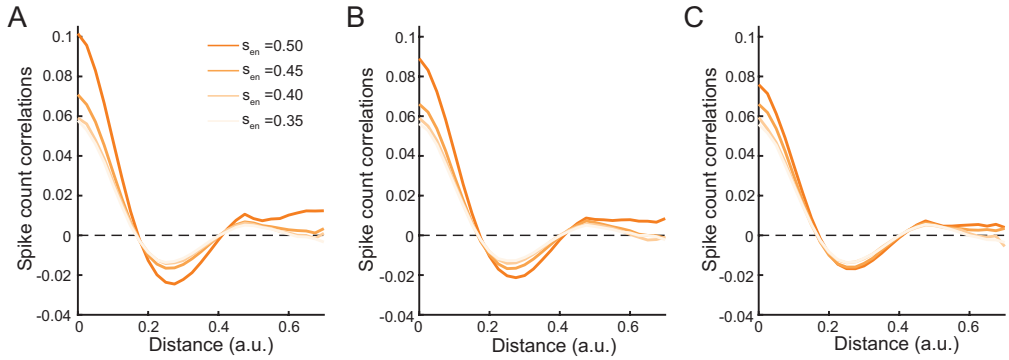

S2 Fig. Spatial correlations as a function of ensheathment parameters. Spike count correlations as a function of distance for different probabilities of ensheathment (A: $p_{en}^{ae} = 0.9$, B: $p_{en}^{ae} = 0.85$, C: $p_{en}^{ae} = 0.8$) and ensheathment strengths ($s_{en} \in [0.35, 0.5]$), where the default network exhibits spatial correlations ($\alpha_{\text{rec}} = 0.2$ and $\alpha_{\text{ffwd}} = 0.1$).

S1 Movie. Movie of spatial raster plot showing tight clusters of spiking neurons. Will be made available upon acceptance for publication.

Acknowledgments

G.H. would like to acknowledge support from the Swartz Foundation Fellowship for Theory in Neuroscience and the Burroughs Wellcome Fund's Career Award at the Scientific Interface. AB would like to acknowledge support from National Science Foundation award NSF-DMS-1853673 and the support and resources from the Center for High Performance Computing at the University of Utah.

Data availability

The code used to generate the computational data will be made available on the GitHub database (https://github.com/gregoryhandy) upon acceptance for publication.

References

1. Ocker GK, Hu Y, Buice MA, Doiron B, Josić K, Rosenbaum R, et al. From the Statistics of Connectivity to the Statistics of Spike Times in Neuronal Networks. Current Opinion in Neurobiology. 2017;46:109–119. doi:10.1016/j.conb.2017.07.011.
2. Rosenbaum R, Smith MA, Kohn A, Rubin JE, Doiron B. The Spatial Structure of Correlated Neuronal Variability. Nature Neuroscience. 2017;20(1):107–114. doi:10.1038/nn.4433.
3. Hu Y, Trousdale J, Josić K, Shea-Brown E. Motif Statistics and Spike Correlations in Neuronal Networks. Journal of Statistical Mechanics: Theory and Experiment. 2013;2013(03):P03012. doi:10.1088/1742-5468/2013/03/P03012.
4. Trousdale J, Hu Y, Shea-Brown E, Josić K. Impact of Network Structure and Cellular Response on Spike Time Correlations. PLoS Computational Biology. 2012;8(3):e1002408. doi:10.1371/journal.pcbi.1002408.
5. Lee WCA, Bonin V, Reed M, Graham BJ, Hood G, Glattfelder K, et al. Anatomy and Function of an Excitatory Network in the Visual Cortex. Nature. 2016;532(7599):370–374. doi:10.1038/nature17192.
6. Kasthuri N, Hayworth KJ, Berger DR, Schalek RL, Conchello JA, Knowles-Barley S, et al. Saturated Reconstruction of a Volume of Neocortex. Cell. 2015;162(3):648–661. doi:10.1016/j.cell.2015.06.054.

7. Helmstaedter M, Briggman KL, Turaga SC, Jain V, Seung HS, Denk W. Connectomic Reconstruction of the Inner Plexiform Layer in the Mouse Retina. Nature. 2013;500(7461):168–174. doi:10.1038/nature12346.
8. Consortium M, Bae JA, Baptiste M, Bodor AL, Brittain D, Buchanan J, et al. Functional Connectomics Spanning Multiple Areas of Mouse Visual Cortex. bioRxiv. 2021; p. 2021.07.28.454025.
9. Špaček J. Three-Dimensional Analysis of Dendritic Spines. Anatomy and Embryology. 1985;171(2):245–252. doi:10.1007/BF00341419.
10. Ventura R, Harris KM. Three-Dimensional Relationships between Hippocampal Synapses and Astrocytes. The Journal of neuroscience : the official journal of the Society for Neuroscience. 1999;19(16):6897–906.
11. Doron A, Rubin A, Benmelech-Chovav A, Benaim N, Carmi T, Refaeli R, et al. Hippocampal Astrocytes Encode Reward Location. Nature. 2022;doi:10.1038/s41586-022-05146-6.
12. Tzingounis AV, Wadiche JI. Glutamate Transporters: Confining Runaway Excitation by Shaping Synaptic Transmission. Nature reviews Neuroscience. 2007;8(12):935–47. doi:10.1038/nrn2274.
13. Anderson CM, Swanson RA. Astrocyte Glutamate Transport: Review of Properties, Regulation, and Physiological Functions. Glia. 2000;32(1):1–14. doi:10.1002/1098-1136(200010)32:1¡1::AID-GLIA10¿3.0.CO;2-W.
14. Covelo A, Araque A. Neuronal Activity Determines Distinct Gliotransmitter Release from a Single Astrocyte. eLife. 2018;7:1–19. doi:10.7554/eLife.32237.
15. Van Vreeswijk C, Abbott LF, Bard Ermentrout G. When Inhibition Not Excitation Synchronizes Neural Firing. Journal of Computational Neuroscience. 1994;1(4):313–321. doi:10.1007/BF00961879.
16. Rajan K, Abbott LF. Eigenvalue Spectra of Random Matrices for Neural Networks. Physical Review Letters. 2006;97(18):188104. doi:10.1103/PhysRevLett.97.188104.
17. Rajan K, Abbott LF, Sompolinsky H. Stimulus-Dependent Suppression of Chaos in Recurrent Neural Networks. Physical Review E. 2010;82(1):011903. doi:10.1103/PhysRevE.82.011903.
18. Mastrogiuseppe F, Ostojic S. Linking Connectivity, Dynamics, and Computations in Low-Rank Recurrent Neural Networks. Neuron. 2018;99(3):609–623.e29. doi:10.1016/j.neuron.2018.07.003.
19. Coulter SC Douglas. Role of Astrocytes in Epilpesy. Cold Spring Harb Perspect Med. 2015;5(a022434):1–13. doi:10.1038/clpt.2011.183.
20. Heneka MT, Carson MJ, Khoury JE, Landreth GE, Brosseron F, Feinstein DL, et al. Neuroinflammation in Alzheimer's Disease. The Lancet Neurology. 2015;14(4):388–405. doi:10.1016/S1474-4422(15)70016-5.
21. Wade J. Self-Repair in a Bidirectionally Coupled Astrocyte-Neuron (AN) System Based on Retrograde Signaling. Frontiers in Computational Neuroscience. 2012;6(September):1–12. doi:10.3389/fncom.2012.00076.
22. Reato D, Cammarota M, Parra LC, Carmignoto G. Computational Model of Neuron-Astrocyte Interactions during Focal Seizure Generation. Frontiers in computational neuroscience. 2012;6(October):81. doi:10.3389/fncom.2012.00081.
23. Huguet G, Joglekar A, Messi LM, Buckalew R, Wong S, Terman D. Neuroprotective Role of Gap Junctions in a Neuron Astrocyte Network Model. Biophysical Journal. 2016;111(2):452–462. doi:10.1016/j.bpj.2016.05.051.
24. Garnier A, Vidal A, Benali H. A Theoretical Study on the Role of Astrocytic Activity in Neuronal Hyperexcitability by a Novel Neuron-Glia Mass Model. The Journal of Mathematical Neuroscience. 2016;6(1):10. doi:10.1186/s13408-016-0042-0.
25. Umpierre AD, West PJ, White JA, Wilcox KS. Conditional Knock-out of mGluR5 from Astrocytes during Epilepsy Development Impairs High-Frequency Glutamate Uptake. Journal of Neuroscience. 2019;39(4):727–742. doi:10.1523/JNEUROSCI.1148-18.2018.
26. Handy G, Lawley SD, Borisyuk A. Role of Trap Recharge Time on the Statistics of Captured Particles. Physical Review E. 2019;99(2):022420. doi:10.1103/PhysRevE.99.022420.
27. Handy G, Lawley SD, Borisyuk A. Receptor Recharge Time Drastically Reduces the Number of Captured Particles. PLOS Computational Biology. 2018;14(3):e1006015. doi:10.1371/journal.pcbi.1006015.
28. Rosenbaum R, Doiron B. Balanced Networks of Spiking Neurons with Spatially Dependent Recurrent Connections. Physical Review X. 2014;4(2):1–9. doi:10.1103/PhysRevX.4.021039.
29. Renart A, De La Rocha J, Bartho P, Hollender L, Parga N, Reyes A, et al. The Asynchronous State in Cortical Circuits. Science. 2010;327(5965):587–590. doi:10.1126/science.1179850.

30. de la Rocha J, Doiron B, Shea-Brown E, Josić K, Reyes A. Correlation between Neural Spike Trains Increases with Firing Rate. Nature. 2007;448(7155):802–806. doi:10.1038/nature06028.

31. Huang C, Ruff DA, Pyle R, Rosenbaum R, Cohen MR, Doiron B. Circuit Models of Low-Dimensional Shared Variability in Cortical Networks. Neuron. 2019;101(2):337–348.e4. doi:10.1016/j.neuron.2018.11.034.

32. Sanzeni A, Histed MH, Brunel N. Emergence of Irregular Activity in Networks of Strongly Coupled Conductance-Based Neurons. 2020; p. 1–37.

33. Li B, Routh BN, Johnston D, Seidemann E, Priebe NJ. Voltage-Gated Intrinsic Conductances Shape the Input-Output Relationship of Cortical Neurons in Behaving Primate V1. Neuron. 2020; p. 1–12. doi:10.1016/j.neuron.2020.04.001.

34. Veit J, Handy G, Mossing DP, Doiron B, Adesnik H. Cortical VIP Neurons Locally Control the Gain but Globally Control the Coherence of Gamma Band Rhythms. bioRxiv. 2021; p. 1–29.

35. Ahmadian Y, Miller KD. What Is the Dynamical Regime of Cerebral Cortex? Neuron. 2021;109(21):3373–3391. doi:10.1016/j.neuron.2021.07.031.

36. Sanzeni A, Akitake B, Goldbach HC, Leedy CE, Brunel N, Histed MH. Inhibition Stabilization Is a Widespread Property of Cortical Networks. eLife. 2020;9:1–39. doi:10.7554/eLife.54875.

37. Clarke LE, Barres BA. Emerging Roles of Astrocytes in Neural Circuit Development. Nature Reviews Neuroscience. 2013;14(5):311–321. doi:10.1038/nrn3484.

38. Handy G, Taheri M, White JA, Borisyuk A. Mathematical Investigation of IP3-dependent Calcium Dynamics in Astrocytes. Journal of Computational Neuroscience. 2017;42(3):257–273. doi:10.1007/s10827-017-0640-1.

39. Taheri M, Handy G, Borisyuk A, White JA. Diversity of Evoked Astrocyte Ca2+ Dynamics Quantified through Experimental Measurements and Mathematical Modeling. Frontiers in Systems Neuroscience. 2017;11(23):1–19. doi:10.3389/fnsys.2017.00079.

40. Larsen BR, Assentoft M, Cotrina ML, Hua SZ, Nedergaard M, Kaila K, et al. Contributions of the Na+/K+-ATPase, NKCC1, and Kir4.1 to Hippocampal K+ Clearance and Volume Responses. GLIA. 2014;62(4):608–622. doi:10.1002/glia.22629.

41. Sloan SA, Barres BA. Looks Can Be Deceiving: Reconsidering the Evidence for Gliotransmission. Neuron. 2014;84(6):1112–1115. doi:10.1016/j.neuron.2014.12.003.

42. Fiacco TA, McCarthy KD. Multiple Lines of Evidence Indicate That Gliotransmission Does Not Occur under Physiological Conditions. The Journal of Neuroscience. 2018;38(1):3–13. doi:10.1523/JNEUROSCI.0016-17.2017.

43. Savtchouk I, Volterra A. Gliotransmission: Beyond Black-and-White. The Journal of Neuroscience. 2018;38(1):14–25. doi:10.1523/JNEUROSCI.0017-17.2017.